American Mineralogist, Volume 84, pages 171–182, 1999

Biologically induced iron ore at Gunma iron mine, Japan

JUNJI AKAI,[1] KURUMI AKAI,[2] MAKOTO ITO,[1] SATOSHI NAKANO,[3] YONOSUKE MAKI,[4] AND ICHIRO SASAGAWA[5]

[1]Department of Geology, Faculty of Science, Niigata University, Ikarashi-2, Niigata 950-2181, Japan
[2]Kamo-gyosei High School, Gakko-cho, Kamo 956-1322, Japan
[3]Department of Earth Science, Shiga University, Otsu 520, Japan
[4]Laboratory of Biology, Faculty of Humanities and Social Sciences, Iwate University, 3-18-34, Ueda, Morioka 020, Japan
[5]Department of Oral Anatomy, Nippon Dental University, Hamaura, Niigata 951-8151, Japan

ABSTRACT

The mineralogy of sedimentary iron ores from the Gunma iron mine are described to evaluate the role of microorganisms and plants in ore formation. The iron ore is composed of nanocrystalline goethite, well-crystallized jarosite and very small amounts of strengite. The ore characteristically occurs as thick-bands of alternating goethite and jarosite bands, thin-bands of different goethite grain sizes, and fossil-aggregate ore rich in moss and/or leaves. Algal fossils are clearly preserved in the goethite bands in the thick-banded ore. Lattice imaging showed characteristic crystallographic orientations of the goethite nanocrystals. The thin-banded iron ores consist of micrometer-sized chestnut-burr-like goethite aggregates, probably formed by bacterial iron biomineralization. The bands may be attributed to biological or seasonal rhythms. Various products of biomineralization are found in the present-day pH 2–3, Fe^{2+}-, and SO_4^{2-}-rich streams. Bacterial precipitation had variations from amorphous Fe-P-(S) precipitates near the outlet of mineral spring to Fe-P-S precipitates and to Fe-S-(P) (schwertmannite-like) precipitates in the midstream. Mosses and green algae are also collecting Fe precipitates in and around the living and dead cells. Comparison of the processes occurring in the present-day streams and the iron-ore specimens supports the interpretation of these ores as the product of biomineralization.

INTRODUCTION

Iron minerals occur widely in various geological environments on the Earth's surface. Iron minerals are often formed by biological processes involving bacteria (Ghiorse and Ehrlich 1992; Ferris et al. 1988; Mann et al. 1992). The Proterozoic is characterized by large iron deposits known as banded iron formations (BIF) (e.g., Meyer 1985). The biotic or abiotic origin of BIF has been debated (Meyer 1985; Holm 1987; Widdel et al. 1993). Stromatolitic iron ore also has been reported (Dai et al. 1996). Fossilized remnants with bacteria-like forms are also reported from Precambrian rocks although they are not BIF (e.g., Cloud 1965; Holm 1987). Microbial iron precipitation requires further evaluation. Small sedimentary iron ore deposits, such as bog iron ore (Pontus 1955; Crerar et al. 1979) or lacustrine Fe/Mn ore (Dubinina 1981) are also known. Some of these are formed by acid groundwater systems or lake water, and a bacterial contribution to their formation is considered likely (Crerar et al. 1979; Dubinina 1981). There are many small ochreous precipitates in acid mine water streams. Such acid waters contain schwertmannite, $Fe_{16}O_{16}(OH)_y(SO_4)_z nH_2O$ ($16\text{-}y = 2z$ and $2.0 \leq z \leq 3.5$) which is typically poorly crystalline (Bigham et al. 1990, 1994, and 1996). Other phases have very low crystallinities and their mineralogical characterizations have not been fully established.

Japan has many characteristic volcanism-related iron ores, including very small-scale sedimentary bog-iron ores. Their formation ages are recent (within the last few tens of thousands of years), and in some cases, ore formation continues today. The Gunma Iron Mine is the largest sedimentary iron-ore deposit in Japan. Such sedimentary iron ores long have been considered to be fundamentally inorganic in origin (Saito 1949; Pontus 1955; Honda 1956; Ichikuni 1966). The ores commonly contain plant fossil aggregate, and diatoms (Saito 1949; Honda 1956; Ijiri 1968). Preliminary results mainly dealing with the role of the plants and algae on the formation of iron ores have been reported (Akai et al. 1997a and 1997b). However, it is unclear whether the fossilized organisms have played an important active role in the Fe hydroxide precipitation, or if they were simply cemented passively into the deposit. This paper describes the mineralogy of ore specimens from the Gunma Iron Mine and the biomineralization occurring in the present-day stream water. It discusses iron mineralization mechanisms and evaluates the biogenic nature of the Gunma Iron Ore.

* E-mail: akai@sc.niigata-u.ac.jp

0003–004X/99/0102–0171$05.00

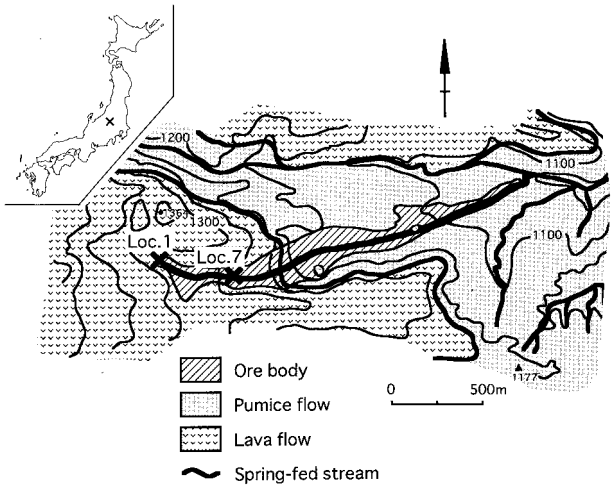

FIGURE 1. Spring-fed stream and sampling sites (Loc. 1 and Loc. 7) plotted on geological sketch map of the study area (modified from Saito 1949). Location of Gunma Iron Mine is indicated in the insert map of Japan.

LOCALITY AND BRIEF SKETCH OF GEOLOGY

The Gunma Iron Mine is located at the eastern foot of the Kusatsu Shirane Volcano in Gunma Prefecture, central Japan (N36 °34′; E138 °30′). Figure 1 indicates spring-fed stream and sampling localities on a simplified geological map. Kusatsu Shirane is an active volcano surrounded by many hot springs. The rocks of this area are predominantly recent andesitic materials (lava-flows, dykes, and pyroclastic sediments). The ore body extends over 2 km along a valley bottom and has a maximum thickness of about 20 m. A spring-fed stream flows through the largely worked-out ore body.

EXPERIMENTAL PROCEDURES

Sample collection

The distributions and characteristics of the various types of iron ore were surveyed in the field. About 300 specimens were sampled from various localities. Mineral spring water was collected in polyethylene bottles. In situ measurements of temperature (T), dissolved oxygen (DO), pH, electric conductivity (EC), and oxidation reduction potential (ORP) in the mineral spring water stream were made. The DO meter is model Tox-90i, Toko Chemical Laboratory Co., Ltd. pH-ORP meter used is pH meter, model Tpx-90i, Toko Chemical Laboratory Co., Ltd. pH meter of D-13. HORIBA Co. was also used. Oxidation-Reduction Potential was obtained by adding corresponding potential values of reference electrode (Ag AgCl 3.3M KCL) to the measured values. EC conductivity meter is Twin Conductivity model B-173, Horiba Co., Ltd. Organisms were collected from sediments and water. Formalin was added to some specimens as a fixative solution.

Sample preparation and analysis

About 100 petrographic thin sections were prepared for light microscopy (LM). Scanning electron microscopy (SEM) observations were carried out by both low vacuum SEM (LVSEM) and high-resolution SEM (HRSEM), using a JSM-5310LVB (JEOL). X-ray electron microprobe analysis (EPMA) mapping was carried out at Shiga University, using a JXA 8800EPMA (JEOL), operating at 15 kV and 2×10^{-8}A beam current. Focused beam and stage scanning methods were used. X-ray diffraction analyses (XRD) were carried out using a Rigaku Geigerflex (Rad-X system). Fe and Cu targets were used. Specimens for transmission electron microscopy (TEM) observations were prepared either by drying suspended material onto a carbon-coated microgrid or by ion thinning of thin-section samples. Soft sediments or soft specimens containing organisms were embedded in an epoxy resin and then thin sectioned by ultramicrotomy. Ion thinning to achieve electron transparency was carried out using a Gatan ion thinning machine model 600N. TEM and high resolution TEM (HRTEM) observations were carried out using a JEM 200CX (JEOL) operating at 200 kV. EDS analyses were carried out by using Voyager IV and TN 2000, Noran Instruments. Co., Ltd.

LM, TEM, and SEM were also used for observation of the biologic specimens. Ultra thin sections of organisms for TEM observation were prepared by diamond microtoming after embedding in an epoxy resin. Phosphate buffer (Millonig) was used.

The stream water samples were immediately filtered after collection through a 0.2 μm membrane filter [type ADVANTEC (cellulose nitrate), Toyo Roshi Co, Ltd., Japan] and the filtered waters were stored in polyethylene bottles for chemical analyses.

Water samples were analyzed in the chemical laboratory of the Research Institute for Hazards in Snowy Areas, Niigata University by N. Watanabe. Chemical analyses include pH, Na^+, NH_4^+, K^+, Mg^{2+}, Ca^{2+}, Fe^{2+}, total Fe, Cl^-, and SO_4^{2-}. Na^+, NH_4^+, K^+, Mg^{2+}, Ca^{2+}, Cl^-, and SO_4^{2-} were measured by an ion chromatography (HIC-6A. Shimadzu Co.). Fe^{2+} and total Fe measurements were made by the o-phenanthroline calorimetric method using a spectrophotometer (Ultraspec 3000. Pharmacia Biotech Co.).

RESULTS

Characteristics of the iron ore

The Gunma Iron Ore is layered or lens-like, and the specimens vary in appearance. The color is typically dark brown or brown, but occasionally, reddish brown. The iron ore is mainly composed of goethite and jarosite in variable proportions, and jarosite is enriched in the upper level of the ore, near the outlet of the mineral spring (Saito 1949). Apparent hardness scale of the goethite-rich ore is 2½–3.

The ore specimens characteristically occur as several types: thin-banded iron ore type (Fig. 2a), thick-banded

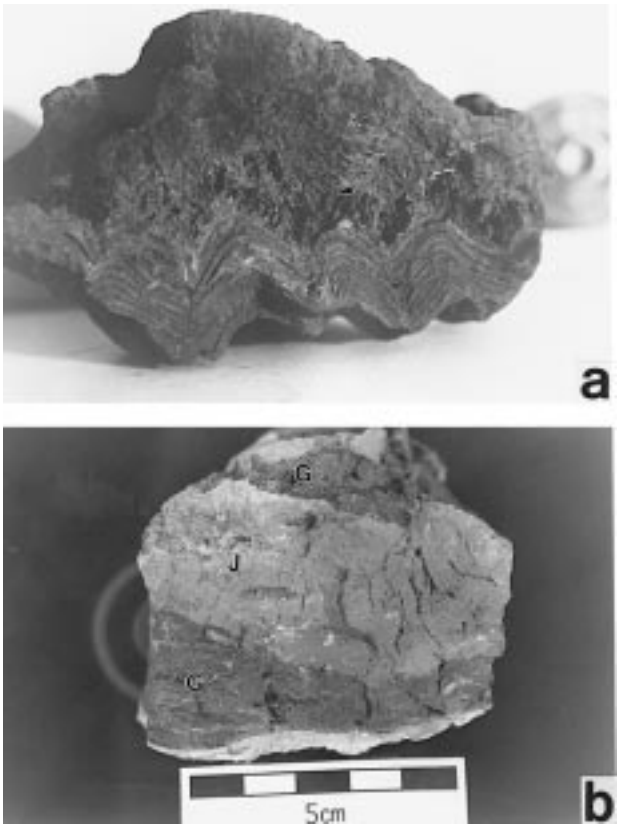

FIGURE 2. Ore types: (**a**) thin-banded; (**b**) thick banded. Specimen height of (**a**) is about 5 cm. Small moss-aggregate ore associated on the thin-banded ore in the photo (**a**) is shown by an arrow. Thick bands in (**b**) are composed of goethite- and jarosite-rich (G and J, respectively) bands.

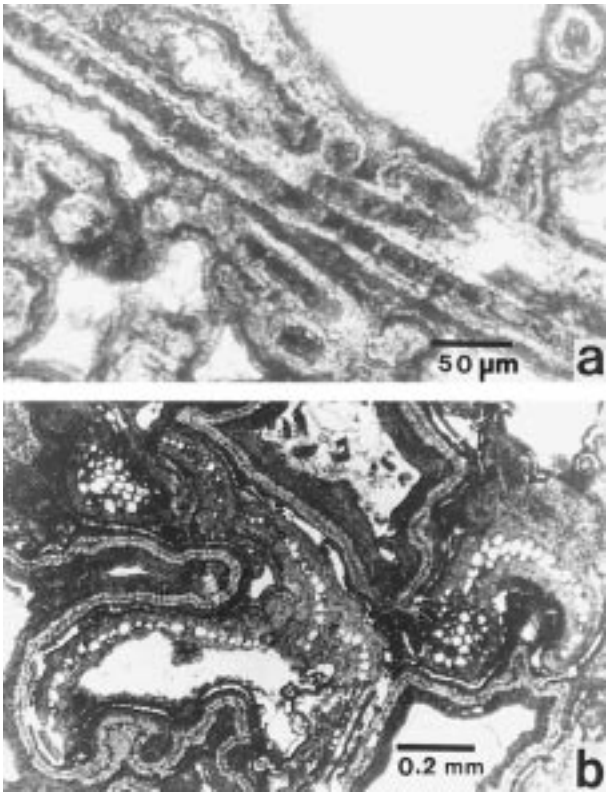

FIGURE 3. Optical micrographs of ore-specimen used for TEM observation. (**a**) Algal aggregates in thick-banded iron ore. (**b**) Moss-aggregate ore. Plant texture is shown by an arrow.

(massive) iron ore (Fig. 2b), submetalic-luster ore, aggreagate ore of moss (or leaf)-like fossils, pumice-rich ore, and others. This study concentrated on the thin-banded, thick-banded and moss-aggregate ores.

LM observation. The thin-banded type (Fig. 3a) shows rhythmic bands composed of fine grains and relatively coarse grains of goethite. The band width ranges from about 0.1 mm to 2 mm. The thick-banded type (Fig. 2b) consists of alternating goethite-rich and jarosite-rich bands of 1–3 cm in thickness. Aggregates of well-preserved, algal-like fossils are common (Fig. 3a). They are similar in shape to several types of green algae noted in the present-day stagnant stream water, one of which may be *Zygnematales* sp. Alternatively, they may be cyanobacteria, such as of *Lyngbya* or *Oscillatoria* (K. Inoue, of Tsukuba University and Quigyu Wu of Tsinghua University, personal communication). The mineralized fossils preserved as goethite usually carry jarosite overgrowths. In some of the goethite-rich layers well preserved casts of leaves, stems or roots of living forms of plants are found (Fig. 3b).

SEM observations. The thin-banded iron ore has a few micrometer-sized spherical chestnut-burr-like mineral aggregates (Fig. 4a). The thick-banded iron ore is composed of tube-like materials (Fig. 4b), in which the tubes are made up of thin, concentric mineral layers. Jarosite crystal aggregates in the thick-banded ore are shown in Figure 4c. Diatom fossils are present in these ores.

XRD data. All the iron ores have only very small broad peaks, around 0.42 nm, 0.27 nm, 0.25 nm, and 0.17 nm, which correspond to 110, 130, 111, and 221 diffractions of goethite (α-FeOOH), respectively. The peaks widths indicate a nanocrystalline grain size or poor crystallinity. The goethite is often associated with variable amounts of jarosite [$KFe_3(SO_4)_2(OH)_6$]. The jarosite XRD peaks are sharp in all the specimens that contain appreciable amounts of jarosite. No other crystalline phases were identified by XRD.

EPMA mapping analyses. The main elements in the bulk iron ore are Fe, S, O, and K (Saito 1949). Figures 5a and 5b show the micrometer-scale distributions of Fe and S in the thin-banded ore, respectively. Iron contents are higher in the thin-banded ore than in the other ore types. Figures 5c and 5d show the Fe and S distribution in the thick-banded algal-aggregate ore. The Fe distribution correlates with the algae forms. As and V distribution patterns were positively correlated with Fe distribution, and S and K are correlated inversely with Fe. S and K may correspond to jarosite-grain distributions, suggesting

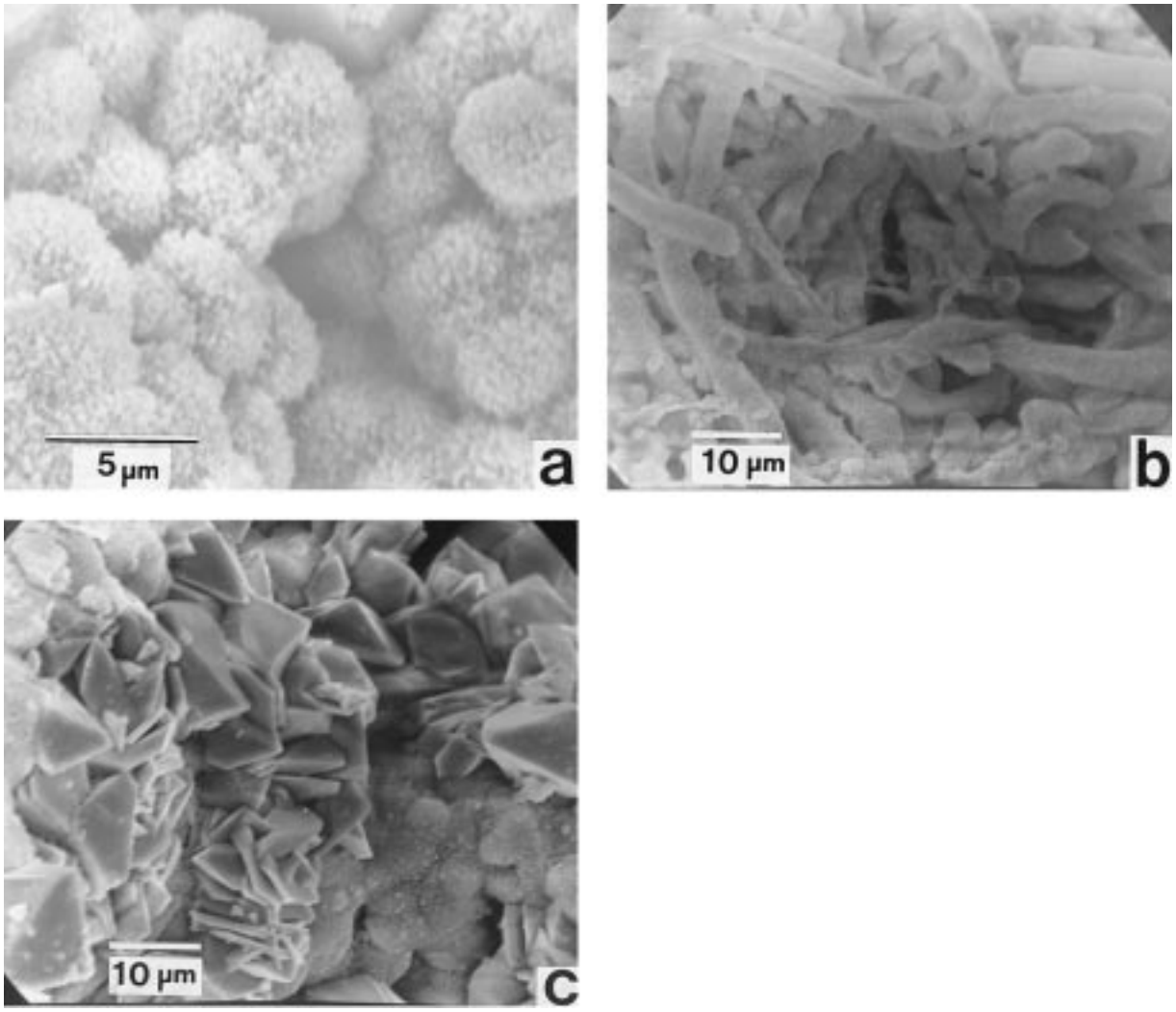

FIGURE 4. SEM images of iron ores. (**a**) Thin-banded ore: Aggregates of small ball-like spherical grains. (**b**) Goethite-rich part in thick-banded ore: Algae-like forms are found. (**c**) Platy crystals of jarosite in the thick-banded ore.

that goethite is inversely correlated to jarosite abundance. The moss-like fossil structures in the aggregate ore are clearly shown by Fe distribution patterns (Figs. 5c and 5f).

TEM observations. The thin-banded ore is characteristically composed of aggregates of small spherical ball-like goethite grains. They are mostly 1–2 μm in diameter, as noted in the SEM examinations. Ion-thinned specimens containing algae-shaped fossils show the diameters of the sheath-like materials to be 30–50 μm. Horizontal sections of the elongated fossils show rounded-rectangular, algae-cell structures. Figure 6a shows a vertical section through an algae-like structure. Goethite was a major phase in the portion of Figure 6a. SAED patterns from goethite are usually characterized by concentric rings or sometimes arcs, suggesting that the crystal grains are in random or semi-random crystallographic orientations. The goethite aggregates display various textures. There are dark (thick mineralized) layer (D in Fig. 6a) and rhythmic light band textures of micrometer sizes (L_1 and L_2 in Fig. 6a). In the light bands, homogeneous layer (L_2), which is relatively rich in carbon, surrounds a central dark portion (D in Fig. 6a). The light contrast band (L_2) is interpreted here as cell-wall structure. The chemical form of carbon is not known.

Figure 6b shows a TEM image of a typical specimen of moss-like and leaf-like fossil aggregate ore. Plant cell-like textures are present. Ring SAED patterns characteristic of goethite suggest a random distribution of small goethite grains. Other iron ore types were examined, and complex textures, mostly mixtures of goethite and jarosite, were observed.

HRTEM observation. Goethite from the algae-like fossils in the thick-banded iron ore is characterized by ring or arc SAED patterns (Figs. 7a and 7b). A HRTEM image of goethite from the light contrast band (L_2) in the

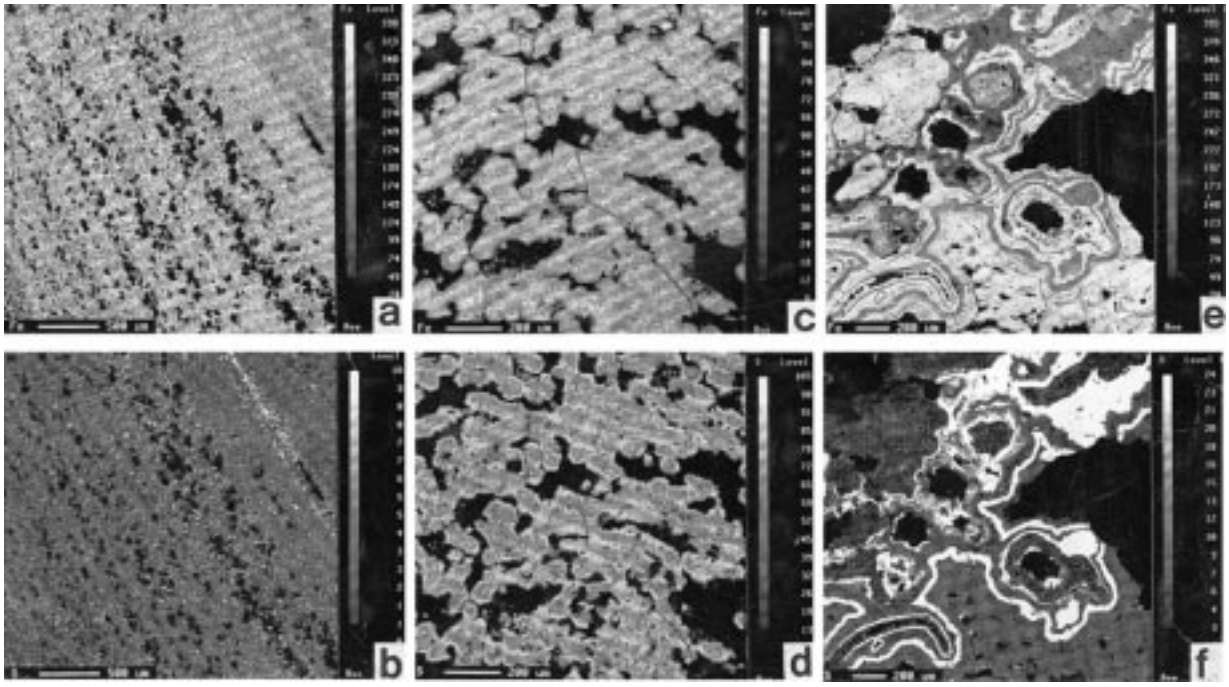

FIGURE 5. Area analysis of elemental distribution by EMPA. Fe (**a**, **c**, and **e**) and S (**b**, **d**, and **f**) distributions of three ore types are shown. Light contrast corresponds to higher concentration. (**a** and **b**) Thin-banded ore. (**c** and **d**) Thick-banded ore. (**e** and **f**) Moss-aggregate ore.

thick-banded ore is shown in Figure 7a. Goethite crystals are commonly about 10–20 nm in diameter. The lattice images display fringes of 0.5 nm and 0.42 nm, which correspond to (020) and (111) planes of goethite, respectively. The crystallographic orientations of the goethite nanocrystals are not random, but show slightly preferred orientations over small distances. Ring SAED patterns are obtained from wider areas. Figure 7b shows the goethite from light (L_2) and dark (D) contrast parts of fossilized algae-like structure in the thick-banded ore although the boundary is not clear. Crystal sizes in D are slightly larger than those in L_2. Locally, SAED patterns contain arc 020 diffractions, suggesting some crystallographic preferred orientation.

SAED patterns and HRTEM images of jarosite show it to be coarsely crystalline without defects. Strengite: $FePO_4\ 2H_2O$ (variscite group; orthorhombic) was also observed (Fig. 8). This mineral is easily damaged by electron beam irradiation. AEM analyses revealed small amounts of As in the strengite. This indicates a position close to strengite in the strengite-scorodite ($FeAsO_4\ 2H_2O$) solid-solution series.

Mineralization in the spring-fed stream

Chemistry of stream water. The ore body fills the floor of a valley that was formerly occupied by a stream. The present-day stream, fed by springs, runs along the top of the ore deposit. Localities 1 to 6 are situated between the spring (Loc. 1) and a point about 300 m downstream (Loc. 6). There are small water falls between the two sites, and some stagnant pools adjacent to the stream (Loc. 5 and Loc. 7). Temperature (*T*), pH, ORP, DO, and EC of the water samples measured in the field are shown in Figure 9, together with a profile along the stream. The DO and ORP values increase downstream. T and EC show little variation, and pH gradually increases downstream. Small abrupt changes were observed in the pH, *T*, and EC values, probably due to superimposition of underflow water and reduced conditions in the stagnant, reductive pools. Water samples from Localities 1–7 were chemically analyzed (Table 1). Waters are characteristically SO_4^{2-}-rich and strongly acidic (pH = 2.46–2.96). Fe^{2+} contents were about 20 ppm at Localities 1 and 2. In the stream water Fe^{2+} tends to be gradually oxidized to Fe^{3+}. However, at Localities 5 and 7, in the stagnant areas, Fe^{2+} values increase again slightly.

Mineralization by organisms. Mineralization by organisms in the stream (Loc. 1 to Loc. 7) was examined mainly by LM and TEM. The acid-resistant moss *Jungermannia thermarum* grows in the upper and middle reaches of the stream. New moss grows continuously on the underlying, almost fully mineralized dead moss, in a manner similar to that of coral-reef growth. There are almost no mineralization products, such as ochreous sediments, in the main stream water, but there is abundant mineralization around mosses and microbes.

Figure 10 shows LM photographs of Fe mineral precipitation on moss cells and green algae in the midstream section. Figure10c shows LM photograph of living diatoms and needle-like sulfur crystals at the outlet (Loc. 1).

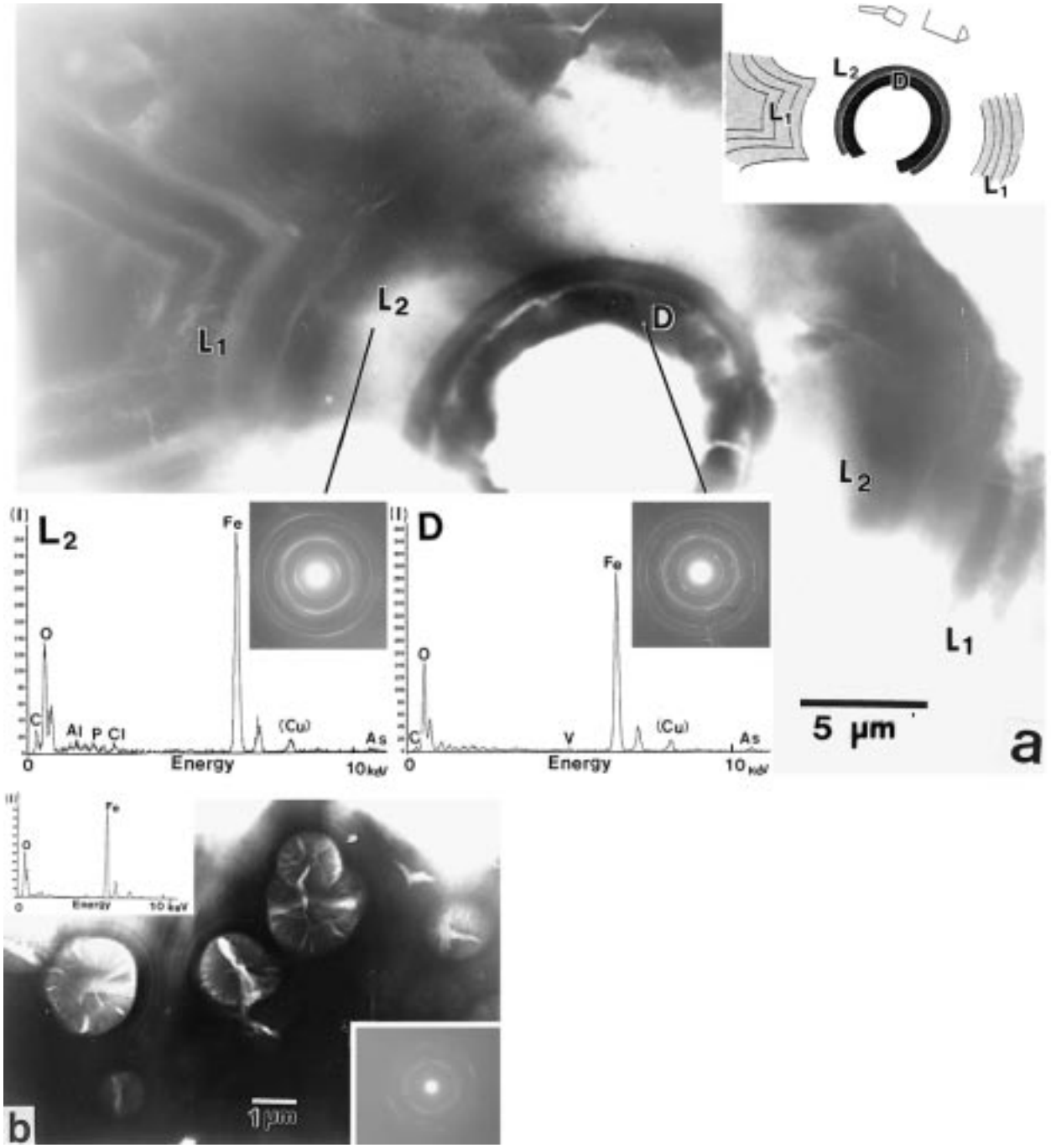

FIGURE 6. TEM images of textures of some ore types. (**a**) Thick-banded ore. Vertical section of algae cells. EDS spectra and SAED patterns corresponding to concentric structures are inserted. Vertical scale in EDS spectra represents characteristic X-ray intensity (I). Label of (Cu) represents peak due to specimen supporting grids and only main peaks are labeled (same also in the following figures). **D** = dark contrast (thick-mineralized) part. $\mathbf{L}_1$ = light contrast part with rhythmic bands. $\mathbf{L}_2$ = homogeneous light contrast part. Schematic explanation of the texture is inserted in the figure. Analytical points are indicated by lines. (**b**) Moss-aggregate ore, showing possible moss textures. SAED pattern and EDS spectrum are inserted.

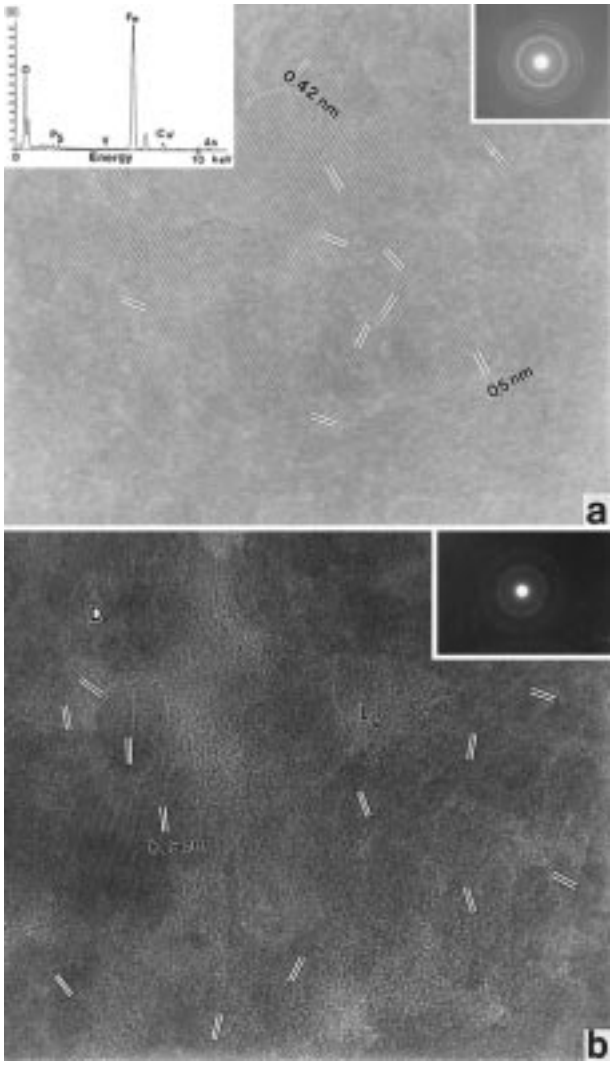

FIGURE 7. HRTEM image of goethite. (**a**) HRTEM image of thick-banded ore. The lattice fringes of 0.5 nm and 0.42 nm correspond to *d* spacings of (020) and (111) planes of goethite, respectively. (**b**) HRTEM image of goethite grains in thick-banded ore. Right hand part corresponds to light contrast part ($\mathbf{L}_2$) and left hand part is thick mineralized part (**D**).

The green, living parts of the moss display no mineral precipitation. The lower part, although it may be still living, is light brownish in color. Lower down, the moss is slightly hardened and is darker brown in color. Under LM observation, iron precipitates occur in and on moss cells (Fig. 10a). Moss at Locality 7 contains variable amounts of Fe precipitates in and around their lower parts. Color changes in the moss cells due to precipitates which were shown by TEM-EDS to be Fe-rich. XRD data of the iron precipitates showed no diffraction peak. SAED pattern analyses of iron precipitates on moss cells showed that the material is nearly amorphous. A specimen from the lower brown part of the moss shows that mineralization is present on the cell wall (Fig. 11).

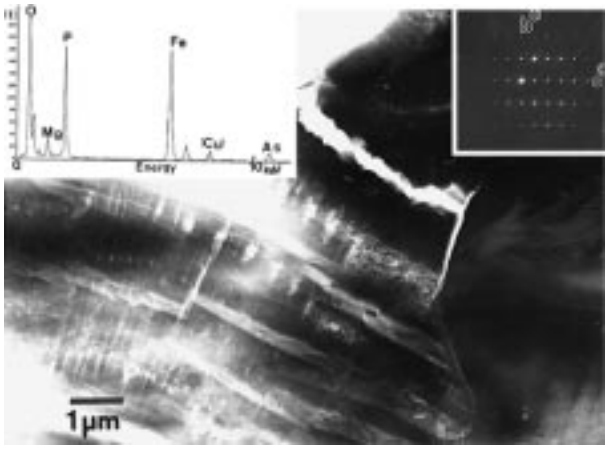

FIGURE 8. TEM image of strengite in thick banded type ore. SAED pattern and EDS spectrum are inserted.

Green algae in the stagnant water (Loc. 7) also precipitate nearly amorphous iron materials in and around their bodies (Fig. 10b). The presence of an Fe component in the precipitates has been confirmed by TEM-EDS analysis.

The water from the spring outlet (Locs. 1 and 2) contains many diatoms. The predominant diatoms are *Eunotia pectinalis* and *Pinnularia Brauni*, the latter being more abundant. Opaque or brownish materials occur in and around the diatoms under the LM (Fig. 10c). TEM, SAED, and TEM-EDS analyses showed that the dark materials are nearly amorphous Fe-P precipitates that contain small amounts of S. The Fe/P ratios of peak heights in the EDS spectra were about 3/2 to 1/1.

At Localities 1 and 2 sulfuric odor is present (H_2S and PO_4 were not measured) and the sediments are sulfur-rich. The presence of orthorhombic sulfur was confirmed by TEM, SAED and EDS analyses. Sulfur aggregates in the TEM image (Fig. 12a) appear to be cemented, probably by some organic matter. It is not clear whether this sulfur is biogenic or nonbiogenic. The bacterial precipitation of Fe-P-(S) amorphous materials in and around the bacillus-shaped bacterial bodies is common at Localities 1 and 2 (Fig. 12b). Spirillum was rarely found. The characteristics of the Fe-P-(S) materials are the same as those in and around the diatoms.

Mineralization occurred most abundantly in the stagnant-water (Locs. 5 and 7). Bacterial biomineralization in samples from Locality 7 was examined by TEM. Results shown in Figure 13 reveal coccoid and bacillus-shaped bacteria with chestnut-burr-like Fe-S-(P) precipitates. Some smaller chestnut-burr-like precipitates were also found. These do not appear to be related to bacterial cell surfaces. XRD of the precipitates showed no peak. SAED patterns of these Fe precipitates appear to be halo-like suggesting that they are nearly amorphous. However some specimens show very faint and very broad diffraction ring patterns in the halos (Fig. 13). The *d* values of the faint and broad diffraction maxima are roughly 0.32

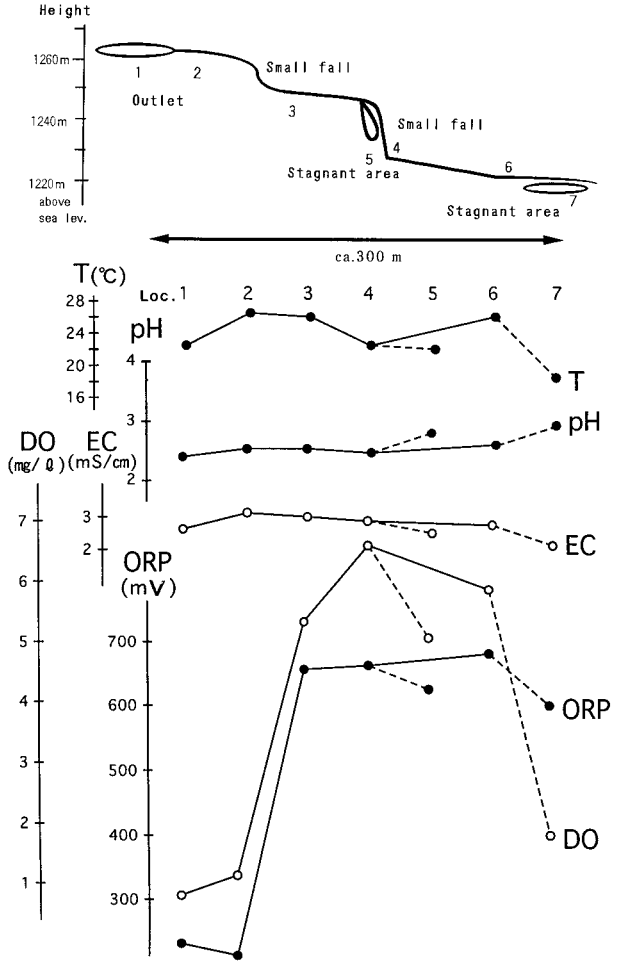

FIGURE 9. Changes of chemical characteristics along the stream. Vertical topographic changes of the stream is schematically shown at the top of the figure. [Loc. 1 = outlet, Loc. 2 = about 10 m apart from Loc. 1 with some additive spring water, Loc. 3 = about 20 m from Loc. 1 (small fall), Loc. 4 = water fall about 5 m high, Loc. 5 = stagnant water adjacent to the fall of Loc. 4, Loc. 6 = stream water about 300 m from the outlet, Loc. 7 = stagnant water adjacent to Loc. 6 where mosses are growing.]

nm, 0.25 nm, and 0.15 nm. These values are similar to those of 310, 212, and 004 diffraction peaks of schwertmannite (Bigham et al. 1994), respectively. The Fe-P-(S) minerals and Fe-S-(P) minerals (P-bearing schwertmannite-like mineral) may be the two extremes, and intermediate type containing Fe, P, and S in variable P/S ratios were found. Culture experiments using water from Locality 7 showed coccus-type and bacillus-shaped bacteria with similar Fe precipitates to be the most characteristic (Akai et al., unpublished manuscript).

Jarosite was not identified although some rare occurrences of amorphous Fe, S, and K minerals at Locality 5 were noted by TEM-EDS analysis. Small amounts of amorphous Fe-hydroxide precipitates without S were rarely and exceptionally found farther downstream (about 1 km) at sites diluted by non-spring water.

At Locality 7 a thin oil-like film showing rainbow-like colors occurred on the surface of the stagnant water. TEM-EDS analyses showed the film to contain Fe and S, but no C. P and/or Al are occasionally contained. The membrane thickness was about 50–90 nm under TEM vacuum. Some samples contain rod-shaped bacteria. The SAED pattern of the membrane was almost amorphous but some specimens showed broad diffractions at 0.32 nm, 0.26 nm, 0.17 nm, and 0.15 nm, which are partly similar to those of schwertmannite. Bacteria without iron precipitates are found in the sediments at the bottom of the pool.

DISCUSSION

Evidence for and the characteristics of biogeneity of the iron ores

EMPA mapping has shown that there is a close relationship between the precipitation of goethite and organic structures within the iron ores. The pattern of precipitation of goethite in living organisms corresponds more closely with the microbe structures than does the jarosite distribution. The jarosite precipitation might occur after iron precipitation or jarosite might be the product of transformation of S-bearing Fe precipitates to goethite. The relatively large sizes and well developed crystal forms of the jarosite suggest that it may be abiotic in origin. Spherical aggregates of goethite in the thin-banded ore (Fig. 4) are a little larger in size, but similar in shape

TABLE 1. Chemical analyses* of water samples in parts per million

Samples	Loc. 1	Loc. 2	Loc. 3	Loc. 4	Loc. 5	Loc. 6	Loc. 7
pH	2.47	2.55	2.57	2.57	2.81	2.64	2.96
Cl^-	303.6	419.3	423.0	368.2	388.7	365.8	327.2
SO^{4-}	945.7	1312.8	1308.6	1155.5	1222.7	1150.6	1025.7
Na^+	38.7	52.4	52.1	45.9	49.4	45.9	42.1
K^+	18.9	25.1	26.1	22.7	24.5	22.0	20.9
Mg^{2+}	31.8	53.1	48.0	40.8	47.3	39.4	36.1
Ca^{2+}	97.1	132.1	131.9	116.6	124.1	115.2	107.3
Fe^{2+}	17.8	20.5	15.6	11.4	18.8	8.8	19.7
Fe^{3+}	N.D.	N.D.	5.4	9.8	2.8	14.9	1.6
SiO_2	945.7	1312.8	1308.6	1155.5	1222.7	1150.6	1025.7

* Analyst is N. Watanabe.

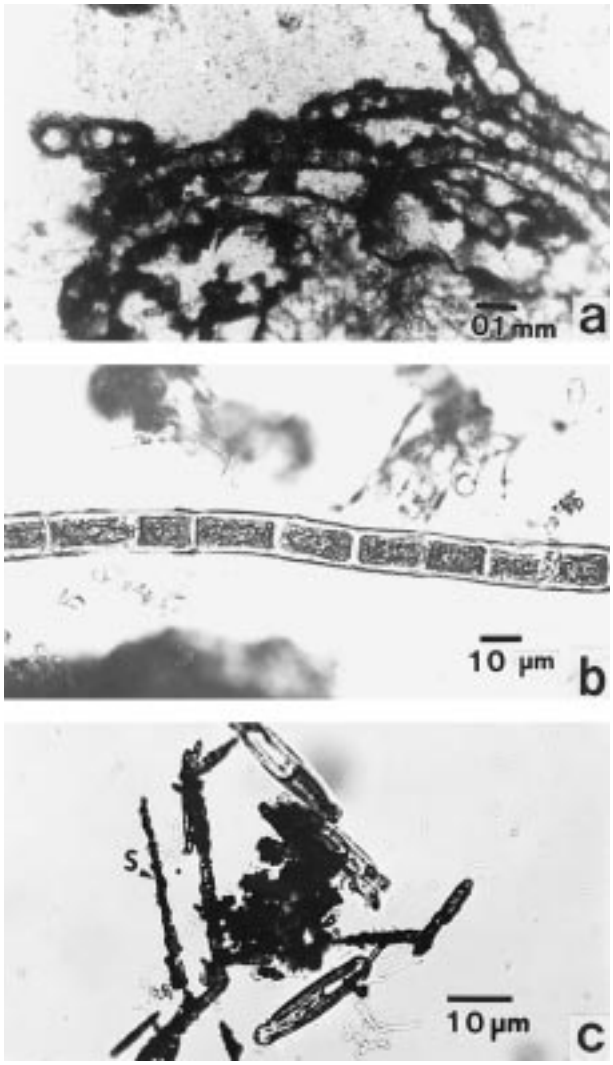

FIGURE 10. LM photographs indicating some examples of biomineralization by mosses, green algae and diatoms in the stream water. (**a**) Moss cells, which are mineralized by almost amorphous iron precipitates. (**b**) Green algae cells in Locality 7. Green algae is also mineralized with iron precipitates. (**c**) Diatoms and sulfur crystals (S) in Locality 1 and 2. Diatom is coated with amorphous Fe-P minerals with small amounts of S in and around the body.

to bacterial iron mineralization. It is suggested here that these goethite aggregates in the iron ore are mainly bacterial aggregates with inorganic overgrowths.

In the thick-banded ore, the dark bands (Fig. 6a) may represent precipitation of nearly amorphous Fe hydroxides, schwertmannite-like mineral, or similar phases on or around algal cells. The finely laminated light contrast bands (L_1 in Fig. 6a) may represent biological, seasonal, or stream-chemistry-related precipitation rhythms on living algal cells. The homogeneous light contrast part (L_2 in Fig. 6a) may be fossilized cell walls. Lattice imaging, SAED patterns, and other mineralogical characteristics of goethite grains show the iron mineralization (schwertmannite-like minerals, Fe hydroxides, or other similar phases) to have been originally precipitated at very small size. The Fe precipitates might have transformed to nanocrystalline goethite. The preferred orientations of the goethite crystals in very local areas, as observed by HRTEM, may be related to their biogenetic origin. More observations are necessary to examine these processes.

Conditions for precipitation of Fe hydroxides in the stream water

The present-day biomineralization is directly related to the chemistry of the modern stream and spring. This may differ from that of the ancient spring water in which iron ores were formed. The two notable differences are the absence of significant amounts of jarosite in the present-day environments and the absence of sulfur precipitates in the iron ore. Similar diatom assemblages in the past (Saito 1949) and present-day environments, and the ore-mineral characteristics suggest similar formation conditions with low pH, a similar temperature range, and SO_4^{2-}-rich solutions. The predominant diatom, *Pinnularia brauni* is widely distributed in mineral springs with pH values from about 1.7 to 4.0 in volcanic regions in Japan (Negoro 1941). Its optimum temperature range is below 35 °C with an upper limit of 48 °C. *Eunotia* sp. occurs in small numbers in stagnant pools (Locs. 5 and 7). Its presence in water at 24 °C and with pH 2.8 to 3.5 has been reported (Negoro 1941). This suggests that the chemistry of the present-day spring may be similar to that of the ancient spring.

The major Fe mineral in the ore is goethite. In this study, extremely rare Fe-hydroxides, and common schwertmannite-like phase with very low crystallinity were found in the present stream environment. However, schwertmannite is considered to be unstable with respect to goethite under the conditions described by Bigham et al. (1990, 1994, and 1996), and the detailed process by which it changes to goethite is not known. All the varieties of the present Fe precipitates found are with very low crystallinities and the phase relations are not known well.

If we suppose the simplest case that dissolved Fe^{2+} is precipitated as ferric hydroxides under oxidizing and high pH conditions, the saturation concentrations of $[Fe^{3+}]$ greatly depend on pH. In the simple system $[Fe^{3+}] + 3(OH)^- \leftrightarrow Fe(OH)_3$, and $Ksp = 10^{-39}$ (Langmuir 1997), saturated $[Fe^{3+}] = 10^{-3}$ mol/L at pH = 2, and saturated $[Fe^{3+}] = 10^{-6}$ mol/L at pH = 3.

ORP values of about 300 mV near the spring (Locs. 1 and 2) suggest that the water is not particularly oxidative. Fe^{3+} values increase downstream but total concentrations of iron ($Fe^{2+} + Fe^{3+}$) are almost constant. Therefore, Fe^{2+} must be oxidized to Fe^{3+} under slightly higher ORP values. Fe^{2+} is, in general, oxidized to Fe^{3+} by bacteria under relatively acidic conditions (pH = 1.5–3.5) (Tuovinen 1990). The observed ORP values (about 680 mV) approach but do not exceed standard redox potential of

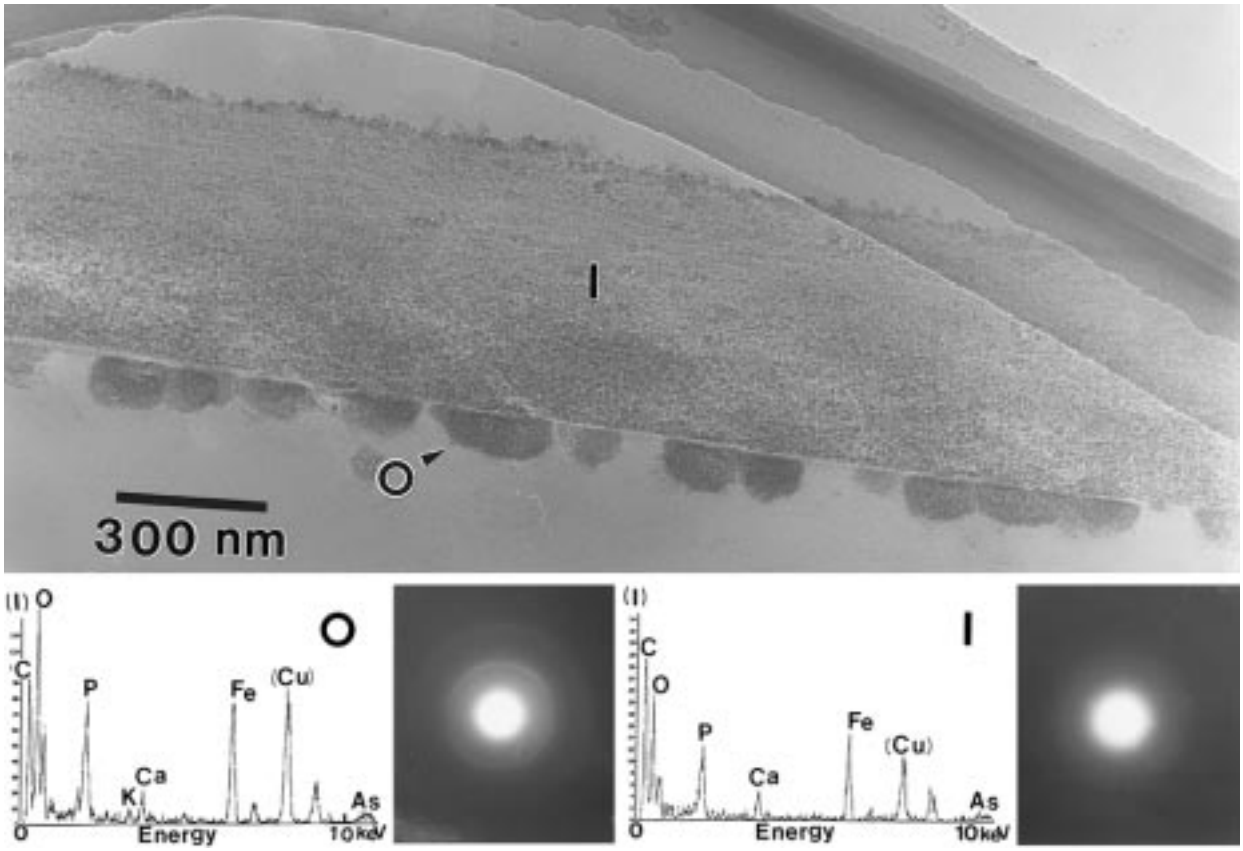

FIGURE 11. TEM image of ultra thin sectioned specimen of moss at Locality 7. O = mineralization outside of the moss cell wall. Nearly amorphous iron minerals are coating on cell wall. Inner cell wall (I) is mineralized to some extent. Corresponding SAED patterns and EDS spectra are inserted. It is not clear whether detected P is due to specimen or to buffer phosphates.

about 730 mV for Fe^{3+}/Fe^{2+} (cf. Brookins 1988; Garrel and Christ 1965). In the pH of the stream water, Fe^{3+} concentrations may approach the solubility of Fe $(OH)_3$, but still not cause precipitation. This may explain apparent absence of inorganic iron-hydroxide (or schwertmannite-like phase) precipitates in the main stream. Otherwise, even if the stream water exceeds the solubility of $Fe(OH)_3$ (or similar phase) locally, the induction period for their precipitation is relatively long under the low supersaturation conditions observed in the stream. The culture experiments in the stagnant water, which was filtered by 0.2 μm membrane to remove microbes showed that schwertmannite or Fe hydroxide precipitation did not occur during a period of a few weeks (Akai et al. unpublished manuscript).

If SO_4^{2-} and K^+ are present, and Fe^{2+} is oxidized to Fe^{3+}, Fe-sulfates (e.g., jarosite) may be formed. Jarosite was not found in the present stream water environments possibly because K^+ is deficient in the present streams.

Biomineralization in the present stream environments

The effects of algae on iron precipitation in the Gunma Iron Ore have been preliminarily reported by Akai (1997a and 1997b). Cyanobacteria and plants in the water may slightly raise the pH on their surfaces during photosynthesis (e.g., Shiraiwa et al. 1993). Such conditions may lead to local saturation and iron precipitation within or outside plant and algae cells in the aqueous environments. The TEM image in Figure 11 in which the inside and outside of the cell walls are mineralized by iron precipitates may relate to this type of iron biomineralization. After the death of the plant, its remains may still act as nucleation sites for further iron mineralization. Finally, the plant tissues may themselves be replaced by Fe precipitates. Inorganic process may also be superimposed on these biomineralization processes and give rise to overgrowths.

The Fe-P minerals with small amounts of S developed near the outlet of the mineral springs (Locs. 1 and 2) may have been formed by the following process: Fe^{2+} is oxidized to Fe^{3+} by bacteria, and amorphous Fe phosphates (or a similar chemical form) are formed using PO_4 ions derived probably from the environment. If this mineral is a phosphate, these may contribute to the strengite recorded in the iron ore. In the stagnant water (Locs. 5 and 7), biomineralization processes predominate. TEM images show various types of microbes coated with iron precipitates. Bacillus- and coccoid-shaped bacteria were com-

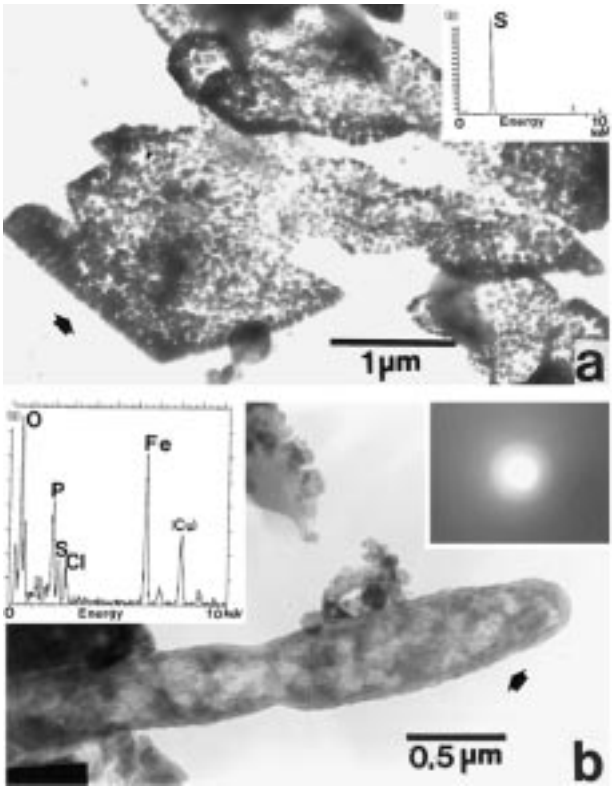

FIGURE 12. TEM images showing present mineralization at Locs. 1 and 2. EDS spectra and SAED pattern are inserted. Analyzed point is shown by an arrow. (**a**) Sulfur crystals (S) which are often surrounded with some substances of probably organic material. (**b**) Bacterial mineralization of Fe-P-(S) minerals on the body.

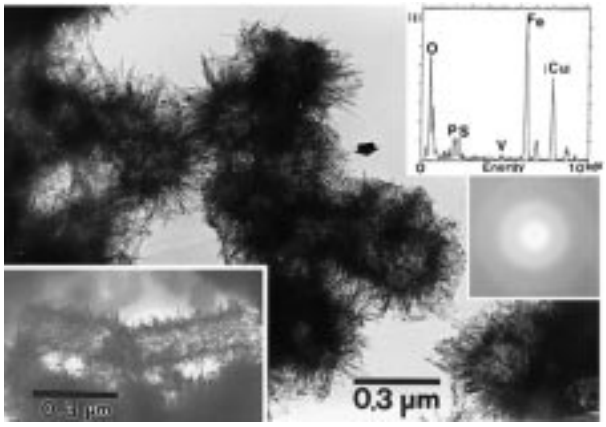

FIGURE 13. TEM images of coccoid -type bacteria at Locality 7. They are coated with Fe-S-(P) precipitates. EDS spectrum and SAED pattern are inserted. Analyzed point is shown by an arrow. TEM image of rod-shaped bacteria coated with Fe-S-(P) precipitates is also inserted in the left bottom corner.

mon. Direct Fe precipitation around bacterial bodies suggests that bacterial effects played an important role in accelerating deposition of the iron ores.

Products of bacterial biomineralization

Types of bacterial precipitation had variations from nearly amorphous Fe-P-(S) precipitates especially near the outlet of mineral spring, to Fe-P-S precipitates and to Fe-S-(P) precipitates. P may be derived partly from bacterial organophosphate compounds. Minerals with compositions between Fe-P-(S) and Fe-S-(P) are nearly amorphous or have low crystallinity, and may be structurally distinct from known phases. The minerals in the surface film on the water may have formed due to bacterial activity. More detailed study is necessary to characterize these phases with low crystallinity.

Characteristics of biologically induced iron ore suggested from present-day biomineralization

The stream waters, and especially the stagnant water, are complex and cooperative ecosystems containing numerous bacteria and other organisms. These give rise to varied microenvironments in which different types of microbe grew and different varieties of iron-mineral precipitate were formed. Comparison of the iron-ore types and the biomineralization has enabled some correlations to be made. The thin-banded ore may be the result of deposition of Fe mineral aggregates of biomineralized coccus-type bacteria. The thick-banded ore may have formed from aggregates of algal fossils. The moss-aggregate ore derives from Fe mineral precipitated on mosses that grew in stagnant water. Iron precipitates around the moss cells in the lower parts of present-day mosses (Figs. 10a and 11). This situation is thought to mimic the process by which this type of iron ore formed. Inorganic precipitation may also be superimposed on the above processes. Biomineralization processes, in general, can be classified into the two types: (BCM) (biologically controlled mineralization) and biologically induced mineralization (BIM) (Lowenstam 1981). BIM processes are characterized by precipitation on and within cells so that the mineral grains have no controlled morphology and size distribution. The results described above suggest that the Gunma Iron Ore is a BIM ore. Bacteria, moss, and algae have probably all contributed to the formation of the iron ore by affecting the local environments in which Fe mineral precipitation occurred.

ACKNOWLEDGMENTS

We thank Jill Banfield of Tokyo University for her critical reading of the manuscript and encouragement. We thank anonymous reviewers for their kind suggestions for improving manuscript. We also acknowledge Keiko Sasaki of Hokkaido University, Naoki Mita of the Geological Survey, Japan, and DeVrinde de Jong of Leiden University for their helpful suggestions on bacterial and algal biomineralization; Naoki Watanabe of Niigata University for chemical analysis of the water samples; Haruo Fukuhara, Iwao Kobayashi of Niigata University, and Yoshihiro Shiraiwa and Kaoru Inoue of Tsukuba University and Quigyu Wu of Tsinghua University and Hiroyuki Yamamoto of St. Marianna University for their help in identification of present and fossilized organisms; Kiyoshi Sawada of Niigata University for his suggestions for chemical principles for precipitations; Kaoru Hoshino of Kokan Kaihatsu Company, Ltd., for his permission of the field study of Gunma Iron Ore area; R.W.Gallois and Tadd

J. Choi of Niigata University for their check of English of the manuscript; and H. Ohfuji of Niigata University for help in drawing figures.

REFERENCES CITED

Akai, J., Kawamoto, K., Akai, K., and Nakano, S. (1997a) Biogenic contribution to the formation of iron ore in Gumma Iron Mine, central Japan. Proceedings of the 30th IGC, 9, 199–208.

Akai, J., Kawamoto, K., and Akai, K. (1997b) Biogenic Iron Ore: TEM Observation of Iron Ore Mineral (goethite) from Gunma Iron Mine. Journal of Mineralogical Society of Japan, 26, 93–97 (in Japanese).

Bigham, J.M., Schwertmann, U., Carlson, L., and Murad, E. (1990) A poorly crystalized oxyhydrosulfate of iron formed by bacterial oxidation of Fe(II) in acid mine waters. Geochimica et Cosmochimica Acta, 54, 2743–2758.

Bigham, J.M., Carlson, L., and Murad, E. (1994) Schwertmannite, a new iron oxyhydroxysulphate from Pyhasalmi, Finland, and other localities. Mineralogical Magazine, 58, 641–648.

Bigham, J.M., Schwertmann, U., Traina, S.J., Winland, R.L., and Wolf, M. (1996) Schwertmannite and the chemical modeling of iron in acid surface waters. Geochimica et Cosmochimica Acta, 60, 2111–2121.

Brookins, D.G. (1988) Eh-pH diagrams for geochemistry. Springer-Verlag, Germany.

Cloud, P.E. Jr. (1965) Significance of the Gunflint (Precambrian) microflora. Science, 148, 27–35.

Crerar, D.A., Knox, G.W., and Means, J.L. (1979) Biogeochemistry of bog iron in the New Jersey Pine Barrens. Chemical Geology, 24, 111–135.

Crist, R.H., Oberholser, K., Shank, N., and Nguyen, M. (1981) Nature of bonding between metallic ions and algal cell walls. Environmental Science and Technology, 15, 1212–1217.

Dai, Y., Cheng, M., Wang, Y., and Shang, J. (1996) Genetic mechanism of Xuanlong Iron deposit in Hebei Province, China. Abstract of the 30th IGC, Beijing. 401.

Dubinina, G.A. (1981) The role of microorganisms in the formation of the recent iron-manganese lacustrine ores. In G. Grasselly, Ed., Geology and geochemistry of manganese, vol. III, p. 305–326. Hungarian Academy of Science, Budapest, Hungary.

Ferris, F.G., Fyfe, W.S., and Beveridge, T.J. (1988) Metallic ion binding by Bacillus subrilis: Implicating for the fossilization of microorganisms. Geology, 16, 149–152.

Garrels, R.M. and Christ, C.L. (1965) Solution, Minerals and Equilibria. Harper & Row Publication Company, New York.

Ghiorse, W.C. and Ehrlich, H.L. (1992) Microbial biomineralization of iron and manganese In H.C.W. Skinner and R.W. Fitzpatrick, Eds., Biomineralization: Processes of iron and manganese, p. 75–99, Catena Verlag, Cremlingen, Germany.

Holm, N.G. (1987) Biogenic influences on the geochemistry of certain ferruginous sediments of hydrothermal origin. Chemical Geology, 63, 45–57.

Honda, S. (1956) A limonitic replacement of a kind of moss. Mining Geology, 6, 29–32 (in Japanese).

Ichikuni, M. (1966) Genesis of the limonite deposits of the Akita iron mine. Mining Geology, 17, 12–15 (in Japanese).

Ijiri, S. (1968) The fossils. Iwanami Shoten Publishers, Tokyo (in Japanese).

Langmuir, D. (1997) Aqueous environmental geochemistry. Prentice Hall Inc., New Jersey.

Lowenstam, H.A. (1981) Minerals formed by organisms. Science, 211, 1126–1131.

Mann, H., Tazaki, K., Fyfe, W.S., and Kerrich, R. (1992) Microbial accumulation of iron and manganese in different aquatic environments: an electron optical study. In H.C.W. Skinner and R.W. Fitzpatrick, Eds., Biominrealization: Processes of iron and manganese, p. 115–132. Catena Verlag, Cremlingen, Germany.

Meyer, C. (1985) Ore metal through geologic history. Science, 227, 1421–1428.

Negoro, K. (1941) Über die allgemeine Verbreitung und das massenhafte Vorkommen von Pinnularia Brauni var. amphicephala (A. Mayer) Hustedt in den mineralogenazidotrophen Gewässern Japans. Proceedings of the Imperial Academy, Vol., XVII no. 9.

Pontus, P.L. (1955) Geochemistry and radio activity of some Mn and Fe bog ores. Geologiska Foereningens Foerhandlingar, 77, 33–44.

Saito, M. (1949) The jarosite-limonite deposit of the Gumma Iron-Mine. Report of Geological Survey of Japan, no.129, 1–30 (in Japanese).

Shiraiwa, Y., Goyal, A., and Tolbert, N.E. (1993) Alkalization of the medium by unicellar green algae during uptake of dissolved inorganic carbon. Plant and Cell Physiology, 34, 649–657.

Tuovinen, O.H. (1990) Biological fundamentals of mineral leaching processes In H.L. Ehrlich and Brierley, Eds., Microbial mineral recovery, p. 55–77. McGraw-Hill, New York.

Widdel, F.S., Schnell, S., Heising, S., Ehrenreich, A., Assmus, B., and Schink, B. (1993) Ferrous iron oxidation by anoxygenic phototrophic bacteria. Nature, 362, 834–836.

MANUSCRIPT RECEIVED MARCH 2, 1998
MANUSCRIPT ACCEPTED AUGUST 26, 1998
PAPER HANDLED BY JILLIAN F. BANFIELD